# Enhancing the electronic and phonon transport properties of two-dimensional hexagonal boron nitride through oxygenation: A first principles study

Basant Roondhe[a,b,*], Vaishali Sharma[b], Hardik L. Kagdada[c], Dheeraj K. Singh[c], Tanusri Saha Dasgupta[a,*], Rajeev Ahuja[d,*]

[a] S.N. Bose National Centre for Basic Science, Kolkata 700098, India
[b] Department of Physics, Faculty of Science, The Maharaja Sayajirao University of Baroda, Vadodara 390002, India
[c] Department of Physics, Institute of Infrastructure Technology Research and Management, Ahmedabad 380026, India
[d] Materials Theory Division, Department of Physics and Astronomy, Uppsala University, Box 516, Uppsala 75120, Sweden

ABSTRACT

Thermoelectric (TE) materials have gathered much attention due to their ability to harvest waste heat energy. To fulfill the goal of sufficient efficiency conversion two important parameters are required (1) low thermal conductivity and (2) high power factor (PF). Two dimensional (2D) hexagonal boron nitride (h-BN) is isostructural with graphene and composed of excellent opto-electronic properties, high mechanical and chemical stability, further exhibiting wide range of applications in diverse areas. Insulating nature of 2D h-BN can be tuned by different approaches such as functionalization, doping or hybrid structures. Therefore, present work focuses on the oxygenation of h-BN, i.e. BNO, for optimization of electronic and phonon transport properties using the state-of-the-art density functional theory (DFT) and Boltzmann transport equation. The presence of oxygen in out-of-plane direction leads to the buckling in h-BN resulting in 65% decrement in the lattice thermal conductivity of BNO (103.66 W/mK) at room temperature. Further, the giant reduction (from 4.63 to 0.7 eV) in electronic bandgap after oxygenation in h-BN is found, leading to the nine times larger electrical conductivity as compared to h-BN. The calculated power factor is almost double in case of BNO. Present study suggests, BNO might have promising utilization in high temperature thermoelectric applications.

## 1. Introduction

The extraordinary properties of graphene, which is a single atomic plane of carbon atoms, have driven an explosion of two dimensional (2D) honeycomb structured materials, exfoliated from their bulk counterparts, such as group IV elements, group III-V, IV-VI and II-VI compounds, which are currently of significant interest due to their unique properties [1–11]. Among all 2D materials, hexagonal boron nitride (h-BN), due to its structural analogy with graphene has gathered much attention [6,12]. The covalent nature of the hetero-nuclear bonding between B and N in the honeycomb lattice of h-BN results in the large bandgap which was missing in graphene [13,14]. However, the large band gap in h-BN restricts the applications for electronic transport and energy conversion, which needs to be reduced. Parallel to the discovery of new 2D materials, motivated by the improved properties of graphene oxide (GO) [15], there has been also attempt on tailoring properties through oxidation, giving rise to a new class of nanomaterials, with wide range of applications [16–18]. For example, very recently, by controlled oxidation, a new material in graphene's group has been developed experimentally named as graphene monoxide (GMO) consisting of quasi hexagonal structure and unusual ratio of carbon and oxygen which is 1:1 in a unit cell [19]. The GMO has semiconducting nature with 0.9 eV bandgap, which might have many electronic applications. Furthermore, the different oxygen and carbon ratio and functional groups in graphene oxide (GO) has been shown to result in wide range of energy gap indicating its possibilities in variety of applications [20–23].

Inspired from the activity on oxidation of graphene and 2D materials, in the present study we explore the effect of oxidation on h-BN, which resulted in the formation of boron nitride oxide (BNO) or "white graphene oxide". Our goal is to achieve the tuning of electronic properties as well as improvement of transport properties for potential
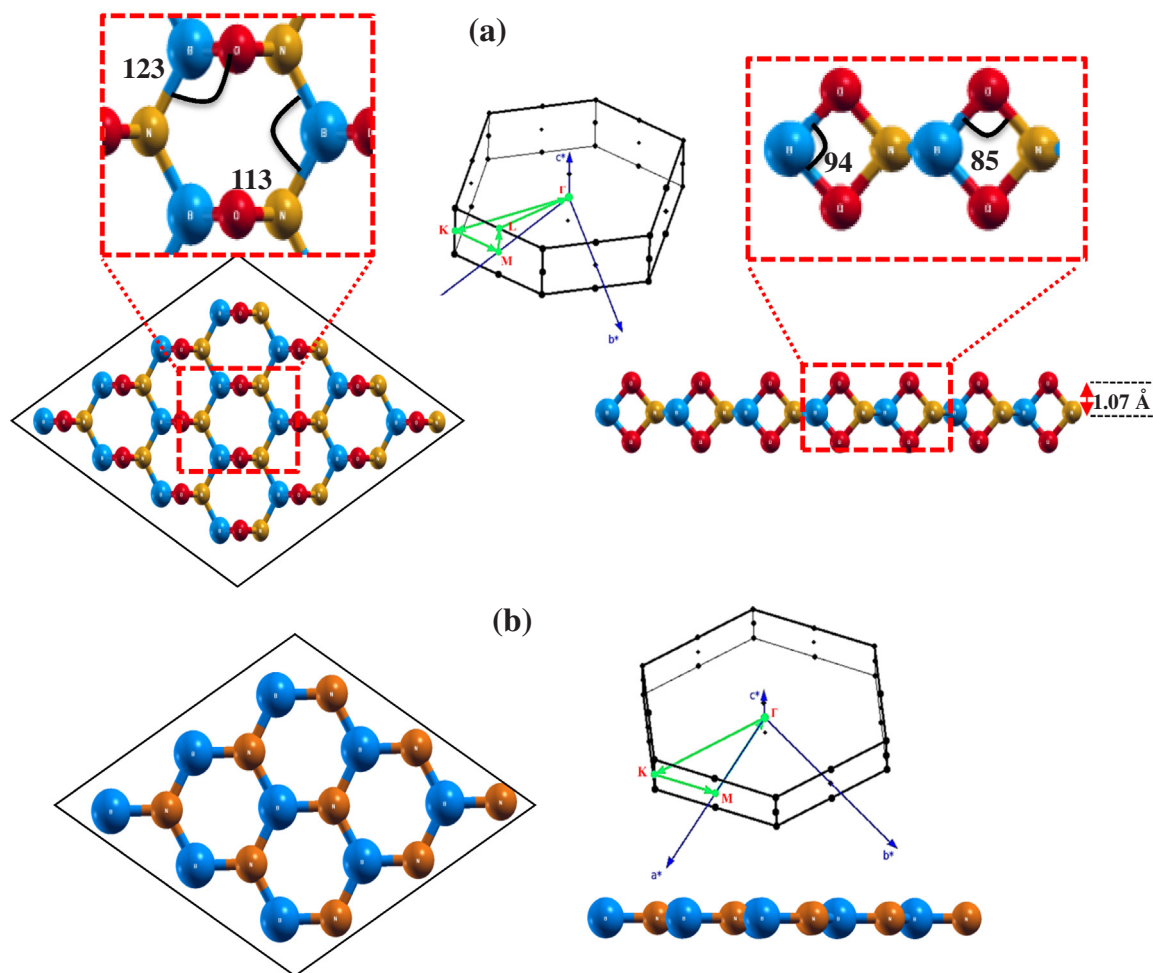
**Fig. 1.** Optimized structure along with their Brillouin zone of (a) BNO and (b) h-BN.

application in thermoelectric device. The thermoelectric (TE) materials have tendency to convert the heat energy into electrical energy. The efficiency of such conversion purely depends on the Seebeck coefficient (S), electrical conductivity (σ), total (electronic and the lattice) thermal conductivity (κ), and temperature (T), which results in the dimensionless quantity figure-of-merit (ZT), expressed as $S^2 \sigma T /\kappa$. The high power factor ($S^2 \sigma$) and low thermal conductivity is essential need for any high efficient thermoelectric materials.

Our first-principles calculations show that the crystal structure of BNO exhibits the buckling which breaks the mirror symmetry. This structural modification of the h-BN might reveal the variety of new and modified properties, introduce the novel era of boron nitride nanostructure. Therefore, we aimed to understand the structural properties, lattice dynamics and electronic properties of 2D materials, as a fundamental point of view. Moreover, the exploration of boron nitride based materials for the application in thermoelectric devices is still limited due to its high thermal conductivity [12]. Some 2D transition metal chalcogenide have gather attention in this regard but it is still in preliminary stage [24]. The buckled structure of BNO with broken mirror symmetry is expected to cause possible enhancement in phonon scattering [25], and promises lower thermal conductivity compared to the graphene [26]. The change in charge carrier and band gap upon oxidation, on the other hand, should influence electrical conductivity and consequently the power factor.

In the present work, we thus investigated the structural, electronic, phonon and TE properties of 2D boron nitride oxide (BNO) or "white graphene oxide" using the combined approach of first-principles method and Boltzmann transport theory. For a deeper understanding of

the results, all the properties are compared with 2D h-BN. For TE properties, we further investigate their temperature dependence, showing the enhancement in power factor from h-BN to BNO.

## 2. Computational method

The structural and electronic properties of h-BN and BNO are investigated using state-of-the-art density functional theory (DFT) based on the first principles calculation. Structural optimizations of h-BN and BNO obtained by employing plane wave method based ultra-soft pseudopotential with generalized gradient approximation (GGA) [27]. All the ground state energy calculations done in QUANTUM ESPRESSO distribution [28]. The convergence in plane wave basis set is achieved with kinetic energy and charge density cutoff of 80 and 800 Ry. During structural optimization, 10x10x1 Monkhorst-Pack [29] k-mesh is used for the sampling of the Brillouin zone (BZ). The total energy of our systems is calculated by Broyden-Fletcher-Goldfarb-Shanno (BFGS) [30] iterative method. The convergence for electronic energy is set to $10^{-8}$ eV and minimum forces between atoms are converged to 0.001 eV/Å. The phonon dispersion is calculated by using density functional perturbation theory (DFPT) implemented in QUANTUM ESPRESSO distribution [31]. To evaluate phonon frequencies precisely, q-mesh of 6x6x1 and 8x8x1 are used for h-BN and BNO, respectively.

The electronic and phonon transport coefficients are calculated by solving both electronic and phonon Boltzmann transport equation separately. The electrical conductivity and electronic thermal conductivity are calculated under rigid-band and constant relaxation time approximation as implemented in BoltzTraP code [32]. The phonon

**Table 1**
Calculated Lattice constant 'a' (Å), Fermi energy 'E_F' (eV), bandgap 'E_g' (eV), bond length (Å) and bond angle (°).

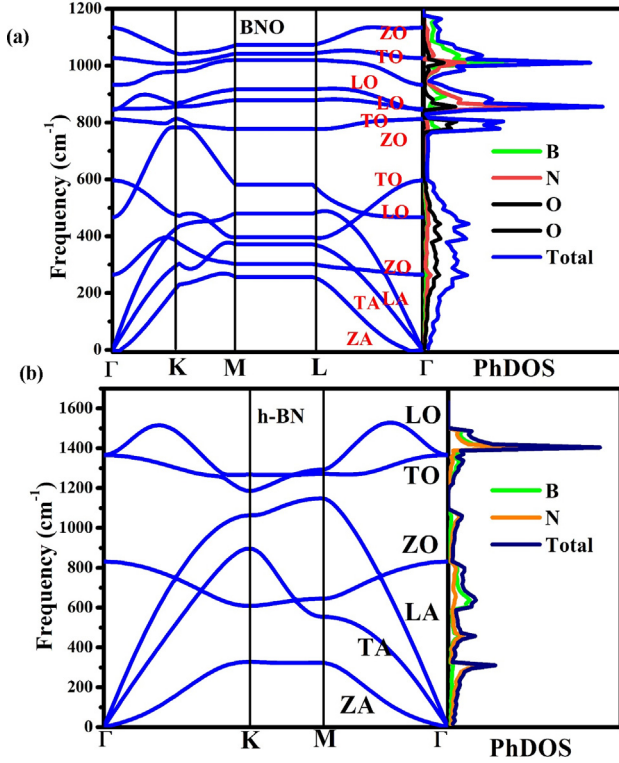| System | $E_F$(eV) | $E_g$ (eV) | Bond length (Å)(B−N) | Bond angle (°) (B−N−B) | Lattice 'a' (Å) |
|---|---|---|---|---|---|
| BNO | −1.18 | 0.7 (Indirect) | 1.98 | 113 | 3.16 |
| h-BN | −3.71 | 4.63 (Direct) | 1.43 | 120 | 2.49 |



**Fig. 2.** Phonon dispersion curve (PDC) along with phonon density of states (PhDOS) of (a) BNO and (b) h-BN.

dependent lattice thermal conductivity is calculated using the following equation [33–34]

$$\kappa_{latt} = \frac{1}{V} \sum_{\lambda} C_\lambda v_{\lambda x}^2 \tau_{\lambda x} \tag{1}$$

where $V$ is the volume of the BZ, $C_\lambda$ is the group velocity of $\lambda^{th}$ phonon mode, $v_{\lambda x}$ and $\tau_{\lambda x}$ determines the group velocity and phonon relaxation time for $\lambda^{th}$ phonon mode along the $x$ direction. The solution of phonon Boltzmann transport equation (PBTE) which is executed in ShengBTE code is utilized to obtained the lattice thermal conductivity using the above expression [35]. This requires two types of force constants: (1) 2nd order interatomic force constant (IFC) which is obtained from DFPT phonon calculations and (2) 3rd order anharmonic IFCs, which is obtained by using supercell approach with a 6x6x1 supercell.

## 3. Results and discussion

### 3.1. Structural and dynamical properties

We start our study with optimization of the structure and lattice constant of both 2D structures h-BN and BNO. The optimized geometries are presented in Fig. 1. The obtained equilibrium lattice constant 'a' of h-BN and BNO, out-of-plane height D of oxygen atom in BNO and bond angle ∠ BNO and ∠ BNB are listed in Table 1. The obtained lattice constants of h-BN and BNO are 2.49 and 3.16 Å, respectively, which is in good agreement with that reported in literature for h-BN [36].
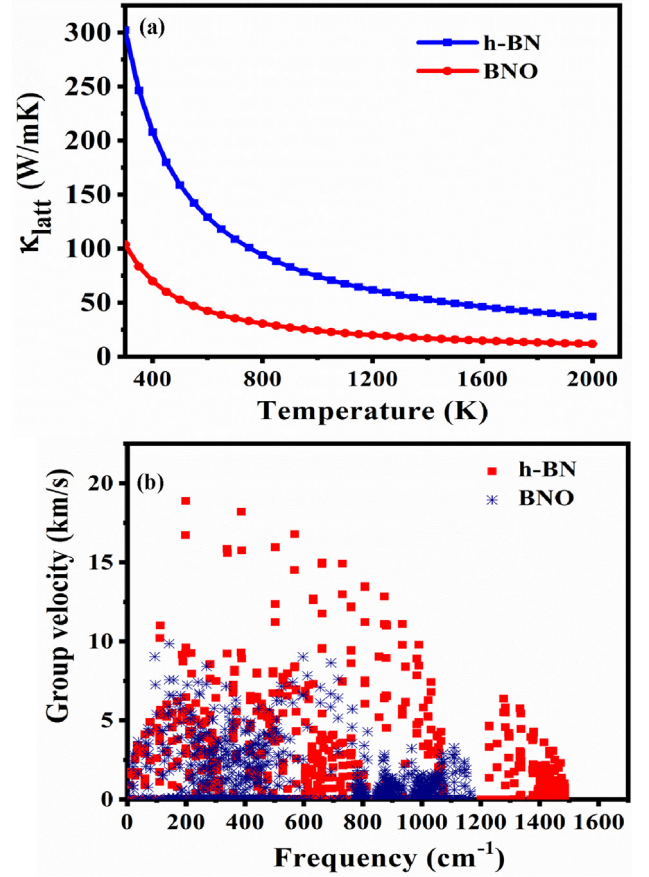


**Fig. 3.** (a) Lattice thermal conductivity ($\kappa_{latt}$) and (b) group velocity of BNO and h-BN.

Further, the presence of oxygen at out of plane position reveals the larger lattice constant of BNO than that of h-BN. The crystal structure of h-BN is hexagonal as in case of graphene, while the BNO shows a highly anisotropic honeycomb crystal structure. The oxygen atom in BNO sits on the bridge site of B-N bonds, 1.07 Å above the plane of B−N, being covalently bonded with B and N, which further increase the bond distance to 1.98 Å from 1.42 Å. This makes the hexagon stretched with one of its six arms formed by buckled B-O-N bonds, and rest four arms formed by B−N bonds. The angle between B−O−N is found to be 85° while the angle between B−N−B becomes 113° contrast to 120° in the case of h-BN. The resulting buckled 3D structure of BNO forms sp²-sp³ hybridized structure in contrast to sp² bonded structure of h-BN.

Due to the peculiar structural properties of BNO compared with its parent h-BN, it is essential to check whether this newly predicted structure is stable in free standing. For this purpose, dynamical stability needs to examined from the calculation of phonon dispersion curves (PDC) in the entire Brillouin zone (Fig. 1). We present PDC of BNO together with the h-BN in Fig. 2. First of all, we notice that phonon frequencies are positive and real in the whole range of BZ, asserting dynamical stability of both the structures. The h-BN and BNO has six and twelve phonon branches, respectively, out of which three are acoustic (A) branches and rest are optical (O) branches. For 2D materials, the main characteristic of phonons is the out-of-plane acoustic mode 'ZA', or flexural mode, which governs the out-of-plane vibrations. Under zero strain condition, the ZA branch follows the quadratic behavior with wave-vector near the zone center, which is the indicator of loss of two-dimensional ordering. Thus, ZA mode is focused widely to understand the rippling in 2D materials [9,37–39]. The frequency of other two acoustic branches: transverse acoustic (TA) and longitudinal acoustic (LA) shows linear behavior near the zone center. BNO phonon
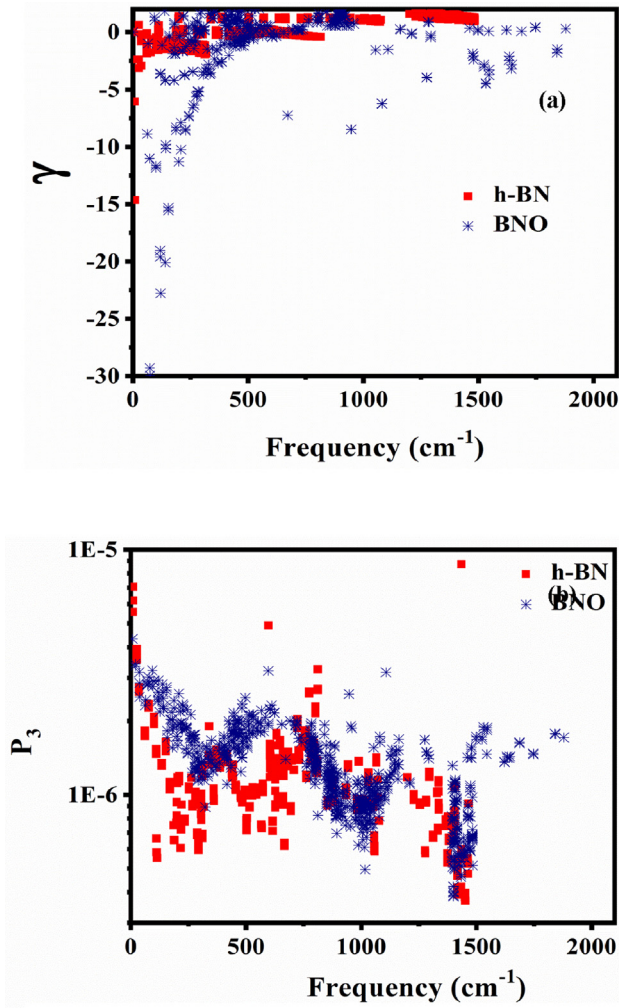
Fig. 4. (a) Grüneisen parameter ($\gamma$) and (b) phase space ($P_3$) of BNO and h-BN.



Fig. 5. Band structure plots and density of states (DOS) of (a) BNO and (b) h-BN.

spectrum show these characteristic features, similar to the h-BN [9,10,14] and graphene [40–41].

In the case of h-BN, out-of-plane vibrations (acoustic and optical section) of PDC have lower frequency compared to other transverse and longitudinal modes. This should be attributed to low dimensionality of the h-BN structure which enforces stronger in-plane bending or stretching of the BN bond compared to the bending in z-direction [37]. In comparison, the BNO phonon dispersion curves bear more three-dimensionality. No frequency gap between LA and ZO modes is observed in both BNO and h-BN due to non-orthogonality of bonds in xy and z directions, leading to finite hybridization between LA and ZO modes. For h-BN, the crossing of LA and ZO modes occur at ~760 cm$^{-1}$ whereas this gets suppressed in BNO to ~270 cm$^{-1}$. Oxidation of h-BN incorporates the additional four branches consisting two bending and two stretching at higher frequency region, illustrating the contribution of oxygen atom in acoustic as well as in optical region of PDC. The atomic-specific contributions to phonon modes can be better understood in terms of projected phonon density of states (PhDOS), as shown in Fig. 2. Because of slightly less mass of boron than nitrogen atom a sharp peak of nitrogen vibrational density of states is observed in acoustic region of h-BN, which suggests a maximum contribution of nitrogen in acoustic phonon modes frequencies. At upper limit of acoustic mode frequencies as well as in the whole optical mode frequencies, both boron and nitrogen atom contribute almost equally in PDCs. On the other hand, in the PDC of BNO, major participation in the acoustic mode frequencies is by oxygen atom. In case of BNO, we observe the presence of oxygen atom in z-direction of sheet leads to
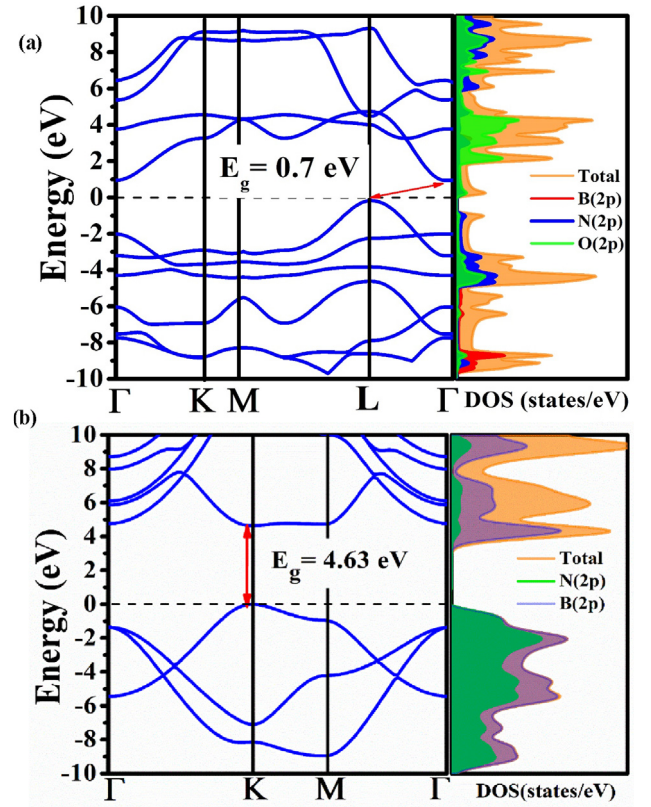
suppression of higher optical vibrational frequencies of boron and nitrogen atoms (1011 cm$^{-1}$ and 857 cm$^{-1}$) compared to that in h-BN (1404 cm$^{-1}$). One should further note from the PDC of BNO that the frequency of acoustic phonon modes is reduced in BNO as compared to h-BN. This reduction in acoustic mode frequencies of BNO can be attributed to the inclusion of oxygen in the unit cell of h-BN, which further diminishes harmonic force constant and increase mass density in BNO [42]. The reduction in phonon frequencies suggests possibility of reduction in lattice thermal conductivity of BNO. The reduced lattice thermal conductivity can be an important parameter for the better thermoelectric performance of a material, as will be discussed in the next section.

### 3.2. Thermal conductivity

The temperature dependent lattice thermal conductivity ($\kappa_{latt}$) of BNO, obtained from the contributions of 2$^{nd}$ order harmonic and 3$^{rd}$ order anharmonic inter atomic force constants and presented in Fig. 3(a) in comparison to that of h-BN. The $\kappa_{latt}$ decreases with the increase of temperature. The room temperature lattice thermal conductivity for BNO is found to be 103.60 W/mK which is almost 1/3$^{rd}$ of the h-BN lattice thermal conductivity (302.33 W/mK).

There can be several factors contributing to the observed large difference in the thermal conductivity between BNO and h-BN, we discuss them in the following.

First of all, as discussed in Section 3.1, there is a reduction in the frequency of acoustic phonon modes in BNO compared to h-BN which would make an important contribution. High values of acoustic frequency near zone center in h-BN also leads to large slope in PDC of h-BN resulting in large group velocity, while for BNO, lower values of acoustic mode frequencies compared to h-BN gives rise to lower group velocity. It is to be further noted that while the group velocity of ZA mode in h-BN and BNO is not notably different, the TA and LA modes
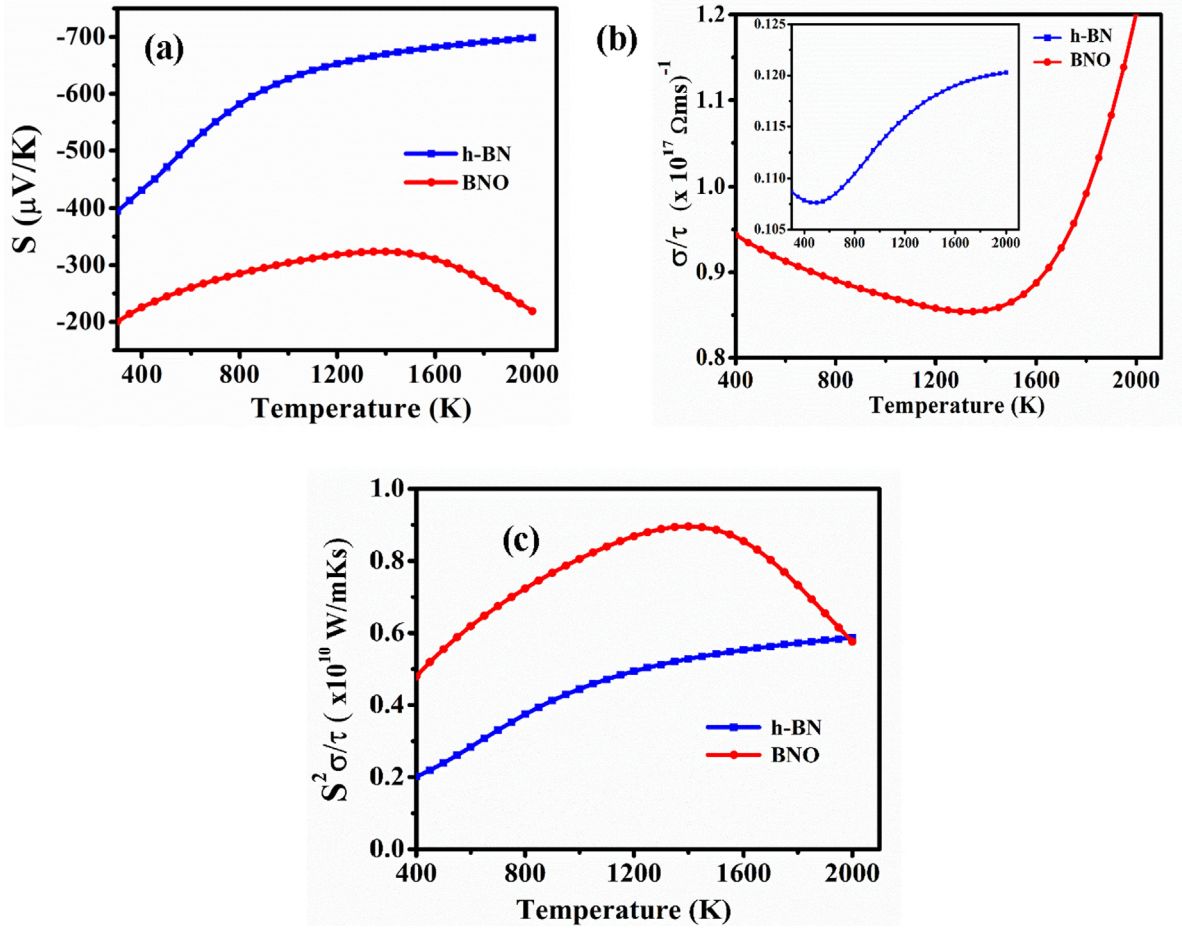
**Fig. 6.** Calculated electronic transport coefficients: (a) Seebeck coefficient (b) electronic conductivity and (c) power factor as a function of temperature (K).

have higher group velocity in h-BN compared to be BNO. This results in lower phonon group velocity in BNO as compared to h-BN, which should contribute in reducing $\kappa_{latt}$ of BNO.

Further, the large anharmonicity in phonon modes would strengthen scattering channels which further contribute in reduction of lattice thermal conductivity [43]. To investigate this possibility, we analyze the phonon mode dependent Grüneisen parameter ($\gamma$), which governs the anharmonicity in phonon modes and potency of scattering paths [40,43]. Negative value of $\gamma$ depicts the weakening of the bonds in crystal structure, while strongest bond has positive value of $\gamma$ in acoustic mode region [44–45]. The frequency dependent, Grüneisen parameters are presented in Fig. 4(a) for h-BN and BNO. As found, the planar, hexagonal structure of h-BN results in nominal anisotropy in properties of h-BN. However, BNO has out-of-plane oxygen atoms in z-direction which increases the anisotropy in this compound leading to large, negative values of Grüneisen parameter. $\gamma$ has more negative value in BNO than in h-BN, which can be attributed to the weaker bonds resulting from increase in bond length between the boron and nitrogen atoms than h-BN.

Moreover, the phase space for three phonon process determines the number of scattering channels which allows phonon scattering with fulfillment of energy and momentum conservations [46–47]. It has also been shown that three phonon process is more dominant than higher order anharmonic scattering process for the lattice thermal conductivity [43,46,48]. Fig. 4(b) shows the phase space ($P_3$) for three phonon process as a function of phonon frequencies for both h-BN and BNO. The inclusion of oxygen atoms in BNO increases the number of atoms in unit cell and hence the phonon branches which governs rules of three phonon scattering more conveniently and leads to a greater number of scattering channels in BNO compared to h-BN. Similar nature of $P_3$ is

found by Wu et al. [49] for hydrogenated graphene. This suggests that the higher value of phase space for the three phonon scattering in BNO, further contributes to low lattice thermal conductivity than h-BN.

### 3.3. Electronic properties and electronic transport

The electronic band structures, calculated along high symmetric direction points in the Brillouin zone **Γ–K–M–Γ** for h-BN and **Γ–K–M–L–Γ** for BNO, are presented in Fig. 5. From the band structure plot, we find that while the h-BN has a large direct bandgap of 4.63 eV, BNO has a small indirect bandgap of 0.7 eV in L–Γ direction. Fig. 5 also shows the total DOS along with PDOS plot for h-BN and BNO. It is clear from the plot that the states near the Fermi level in valence band arises in the case of BNO due to the hybridization occurring between the p orbital electrons of oxygen and nitrogen atoms. The participation of p orbital electron of oxygen thus creates a robust decrement in the bandgap compared to that of large bandgap h-BN. The small bandgap in BNO makes it an interesting material to be explored in the field of thermoelectric application.

Electronic transport properties of a material can be controlled by electronic band structure and density of states. A large electronic band gap gives rise to large value of Seebeck coefficient. Further, the reduction in band gap reveals increment in number of free charge carriers which reduces the Seebeck coefficient [12,34,40,50–52]. In a whole temperature range, we notice that the Seebeck coefficient, as presented in Fig. 6(a), is higher for h-BN than h-BNO which can be attributed to the large electronic band gap in h-BN. While the Seebeck coefficient increases in the whole temperature range for h-BN while, for BNO it first increases up to 1400 K with maximum value of $-323.61$ μV/K and then decreases. The Seebeck coefficient of $-200$ μV/K and $-395$ μV/K

is observed for BNO and h-BN at room temperature respectively. We next evaluate the electrical conductivity under constant relaxation time approximation (CRTA) for both h-BN and h-BNO and present them in Fig. 6(b). It should be noted that in the considered temperature range, electrical conductivity is higher for BNO than h-BN. Here, it is interesting to note that the room temperature electrical conductivity of BNO is around nine times higher than that of h-BN. This significant enhancement in electrical conductivity of BNO is further accounted for the enhancement in power factor, as presented in Fig. 6(c). In most thermoelectric devices, output power is the most important parameter for the efficiency which is determined by the term power factor ($S^2\sigma/\tau$). It is gratifying to note that the formation of BNO by inclusion of oxygen atoms in h-BN doubles the power factor of h-BN. Therefore, present work will be helpful for the enhancement of electronic and phonon transport properties for high efficient heat energy conversion.

## 4. Conclusion

In conclusion, we predicted a new form of hexagonal boron nitride by incorporating the oxygen atom name "white graphene oxide" or BNO. We have investigated the structural, phonon and electronic properties of BNO and found the complete dynamical stability leading to the possibility of synthesizing freestanding BNO. It was found that BNO exists in a highly anisotropic honeycomb crystal structure in contrast to h-BN. Phonon transport properties revealed the reduction in lattice thermal conductivity of BNO as compared to h-BN. The electronic band structure and density of states investigated using the density functional theory shows the transition of large direct bandgap to the indirect bandgap of h-BN after the inclusion of oxygen atom and formation of BNO. The lattice thermal conductivity of BNO was found to be almost one-third of the h-BN. Our calculated power factor reveals that BNO exhibits nine times higher power factor than h-BN. Herein, we propose the role of oxygen in h-BN making it BNO to tune its structural, phonon, electrical and thermoelectric properties and presenting its high potential towards thermoelectric applications.

## CRediT authorship contribution statement

**Basant Roondhe:** Data curation, Formal analysis, Writing - original draft. **Vaishali Sharma:** Methodology, Software. **Hardik L. Kagdada:** Visualization, Investigation. **Dheeraj K. Singh:** Supervision, Validation. **Tanusri Saha Dasgupta:** Conceptualization, Funding acquisition, Resources. **Rajeev Ahuja:** Project administration, Writing - review & editing.

## Declaration of Competing Interest

The authors declare that they have no known competing financial interests or personal relationships that could have appeared to influence the work reported in this paper.

## Acknowledgment

## References

[1] S. Cahangirov, M. Topsakal, E. Aktürk, H. Šahin, S. Ciraci, Two- and one-dimensional honeycomb structures of silicon and germanium, Phys. Rev. Lett. 102 (2009) 236804–236808.
[2] H. Liu, A.T. Neal, Z. Zhu, Z. Luo, X. Xu, D. Tománek, P.D. Ye, Phosphorene: An unexplored 2D semiconductor with a high hole mobility, ACS Nano 8 (2014) 4033–4041.
[3] S.B. Pillai, S. Narayan, S.D. Dabhi, P.K. Jha, First principles calculation of two dimensional antimony and antimony arsenide, AIP Conf. Proc. 1731 (2016) 090024–090027.
[4] S.B. Pillai, S.D. Dabhi, S. Narayan, P.K. Jha, Strain Effect on Electronic and Lattice Dynamical Behaviour of Two Dimensional Bi, BiAs and BiSb, AIP Conf. Proc. 1942 (2018) 090022–090025.
[5] B. Feng, J. Zhang, Q. Zhong, W. Li, S. Li, H. Li, P. Cheng, S. Meng, L. Chen, K. Wu, Experimental realization of two-dimensional boron sheets, Nat. Chem. 8 (2016) 563–568.
[6] A. Pakdel, C. Zhi, Y. Bando, D. Golberg, Low-dimensional boron nitride nanomaterials, Mater. Today 15 (2012) 256–265.
[7] J. Yin, L. Jidong, Y. Hang, Y. Jin, G. Tai, L. Xuemei, Z. Zhang, W. Guo, Boron Nitride Nanostructures: Fabrication, Functionalization and Applications, Small 12 (2016) 2942–2968.
[8] A. Pakdel, Y. Bando, D. Golberg, Nano boron nitride flatland, Chem. Soc. Rev. 43 (2014) 934–959.
[9] P.K. Jha, H.R. Soni, Strain induced modification in phonon dispersion curves of monolayer boron pnictides, J. Appl. Phys. 115 (2014) 023509–023518.
[10] K. Patel, B. Roondhe, S.D. Dabhi, P.K. Jha, A new flatland buddy as toxic gas scavenger: a first principles study, J. Hazard. Mater. 351 (2018) 337–345.
[11] B. Roondhe, P.K. Jha, "Haeckelite" a new low dimensional member of boron nitride family for Biosensing with ultra-fast recovery time: A first principles investigation, J. Mater. Chem. B 6 (2018) 6796–6807.
[12] V. Sharma, H.L. Kagdada, P.K. Jha, P. Śpiewak, K.J. Kurzydłowski, Thermal transport properties of boron nitride based materials: A review, Renew. Sustain. Energy Rev. 120 (2020) 109622–109642.
[13] K.S. Novoselov, D. Jiang, F. Schedin, T. Booth, V.V. Khot-kevich, S. Morozov, A.K. Geim, Two-dimensional atomic crystals, Proc. Natl. Acad. Sci. U.S.A. 102 (2005) 10451–10453.
[14] M. Topsakal, E. Aktürk, S. Ciraci, First-principles study of two- and one-dimensional honeycomb structures of boron nitride, Phy. Rev. B 79 (2009) 115442–115453.
[15] D. Chen, H. Feng, J. Li, Graphene Oxide: Preparation, Functionalization, and Electrochemical Applications, Chem. Rev. 112 (2012) 6027–6053.
[16] K.A. Mkhoyan, A.W. Contryman, J. Silcox, Atomic and electronic structure of graphene-oxide, Nano Lett. 9 (2009) 1058–1063.
[17] S. Park, J. Won Suk, J. An, J. Oh, S. Lee, W. Lee, J.R. Potts, J.-H. Byun, R.S. Ruoff, The effect of concentration of graphene nanoplatelets on mechanical and electrical properties of reduced graphene oxide papers, Carbon 50 (2012) 4573–4578.
[18] G. Lu, S. Park, K. Yu, R.S. Ruoff, L.E. Ocola, D. Rosenmann, J. Chen, Toward practical gas sensing with highly reduced graphene oxide: a new signal processing method to circumvent run-to-run and device-to-device variations, ACS Nano 5 (2011) 1154–1164.
[19] E.C. Mattson, H. Pu, S. Cui, M.A. Schofield, S. Rhim, G. Lu, M.J. Nasse, R.S. Ruoff, M. Weinert, M. Gajdardziska-Josifovska, J. Chen, C.J. Hirschmugl, Evidence of nanocrystalline semiconducting graphene monoxide during thermal reduction of graphene oxide in vacuum, ACS Nano 5 (2011) 9710–9717.
[20] S.D. Dabhi, S.D. Gupta, P.K. Jha, Structural, electronic, mechanical, and dynamical properties of graphene oxides: A first principles study, J. Appl. Phys. 115 (2014) 203517–203527.
[21] J. Yan, L. Xian, M.Y. Chou, Structural and Electronic Properties of Oxidized Graphene, Phys. Rev. Lett. 103 (2009) 086802–086805.
[22] S. Zhang, J. Zhou, Q. Wang, P. Jena, Structure, Stability, and Property Modulations of Stoichiometric Graphene Oxide, J. Phys. Chem. C 117 (2013) 1064–1070.
[23] A. Lerf, H. Heb, T. Riedl, M. Forster, J. Klinowski, 13C and 1H MAS NMR studies of graphite oxide and its chemically modified derivatives, Solid State Ionics 101 (1997) 857–862.
[24] G. Zhang, Y.-W. Zhang, Thermoelectric properties of two-dimensional transition metal dichalcogenides, J. Mater. Chem. C 5 (2017) 7684–7698.
[25] X. Gu, R. Yang, First-principles prediction of phononic thermal conductivity of silicene: A comparison with graphene, J. Appl. Phys. 117 (2015) 025102–025115.
[26] X. Wu, V. Varshney, J. Lee, Y. Pang, A.K. Roy, T. Luo, How to characterize thermal transport capability of 2D materials fairly? – Sheet thermal conductance and the choice of thickness, Chem. Phys. Lett. 669 (2017) 233–237.
[27] J.P. Perdew, K. Burke, M. Ernzerhof, Generalized Gradient Approximation Made Simple, Phys. Rev. Lett. 77 (1996) 3865–3868.
[28] P. Giannozzi, S. Baroni, N. Bonini, M. Calandra, R. Car, C. Cavazzoni, D. Ceresoli, G.L. Chiarotti, M. Cococcioni, I. Dabo, A. Dal Corso, S. De Gironcoli, S. Fabris, G. Fratesi, R. Gebauer, U. Gerstmann, C. Gougoussis, A. Kokalj, M. Lazzeri, L. Martin-Samos, N. Marzari, F. Mauri, R. Mazzarello, S. Paolini, A. Pasquarello, L. Paulatto, C. Sbraccia, S. Scandolo, G. Sclauzero, A.P. Seitsonen, A. Smogunov, P. Umari, R.M. Wentzcovitch, QUANTUM ESPRESSO: A modular and open-source software project for quantum simulations of materials, J. Phys. Condens. Matter 21 (2009) 395502–395521.
[29] H.J. Monkhorst, J.D. Pack, Special points for Brillouin-zone integrations, Phys. Rev. B. 13 (1976) 5188–5192.
[30] J.D. Head, M.C. Zerner, A Broyden-Fletcher-Goldfarb-Shanno optimization procedure for molecular geometries, Chem. Phys. Lett. 122 (1985) 264–270.
[31] S. Baroni, S. De Gironcoli, A. Dal Corso, P. Giannozzi, Phonons and related crystal properties from density-functional perturbation theory, Rev. Mod. Phys. 73 (2001) 515–562.
[32] G.K.H. Madsen, D.J. Singh, BoltzTraP. A code for calculating band-structure dependent quantities, Comput. Phys. Commun. 175 (2006) 67–71.
[33] T. Ouyang, M. Hu, Competing mechanism driving diverse pressure dependence of thermal conductivity of XTe (X=Hg, Cd, and Zn), Phys. Rev. B 92 (2015) 235204–235216.

[34] H.L. Kagdada, P.K. Jha, P. Śpiewak, K.J. Kurzydłowski, Structural stability, dynamical stability, thermoelectric properties, and elastic properties of GeTe at high pressure, Phys. Rev. B 97 (2018) 134105–134115.

[35] W. Li, J. Carrete, N.A. Katcho, N. Mingo, ShengBTE: A solver of the Boltzmann transport equation for phonons, Comput. Phys. Commun. 185 (2014) 1747–1758.

[36] A. Nag, K. Raidongia, K.P.S.S. Hembram, R. Datta, U.V. Waghmare, C.N.R. Rao, Graphene Analogues of BN: Novel Synthesis and Properties, ACS Nano 4 (2010) 1539–1544.

[37] H.R. Soni, P.K. Jha, AIP Adv. 5 (2015) 107103–107108.

[38] J. Hua, G.M. Vanacore, A. Cepellotti, N. Marzari, A.H. Zewaila, Rippling ultrafast dynamics of suspended 2D monolayers, graphene, Proc. Natl. Acad. Sci. U.S.A. 113 (2016) 6555–6561.

[39] F.Q. Wang, J. Yu, Q. Wang, Y. Kawazoe, P. Jena, Lattice thermal conductivity of penta-graphene, Carbon 105 (2016) 424–429.

[40] H.L. Kagdada, P.K. Jha, P. Spiewak, K.J. Kurzydłowski, Understanding the behavior of electronic and phonon transports in germanium based two dimensional chalcogenides, J. Appl. Phys. 124 (2018) 235701–235711.

[41] S.K. Gupta, H.R. Soni, P.K. Jha, Electronic and phonon bandstructures of pristine few layer and metal doped graphene using first principles calculations, AIP Adv. 3 (2013) 032117–032132.

[42] E.N. Koukaras, G. Kalosakas, C. Galiotis, K. Papagelis, Phonon properties of graphene derived from molecular dynamics simulations, Sci. Repo. 5 (2015) 12923–12931.

[43] L.F. Huang, P.-L. Gong, Z. Zeng, Phonon properties, thermal expansion, and thermomechanics of silicene and germanene, Phys Rev. B 91 (2015) 205433–205438.

[44] L.A. Falkovsky, Symmetry constraints on phonon dispersion in graphene, Phys. Lett. A 372 (2008) 5189–5192.

[45] B. Peng, H. Zhang, H. Shao, Y. Xu, G. Ni, R. Zhang, H. Zhu, Phonon transport properties of two-dimensional group-IV materials from *ab initio* calculations, Phys. Rev. B 94 (2016) 245420–245432.

[46] L. Lindsay, D.A. Broido, Three-phonon phase space and lattice thermal conductivity in semiconductors, J. Phys.: Condens. Matter 20 (2008) 165209–165214.

[47] L.F. Huang, T.F. Cao, P.L. Gong, Z. Zeng, Isotope effects on the vibrational, Invar, and Elinvar properties of pristine and hydrogenated graphene, Solid State Commun. 190 (2014) 5–9.

[48] N. Mounet, N. Marzari, First-principles determination of the structural, vibrational and thermodynamic properties of diamond, graphite, and derivatives, Phys. Rev. B 71 (2005) 205214–205228.

[49] X. Wu, V. Varshney, J. Lee, T. Zhang, J.L. Wohlwend, A.K. Roy, T. Luo, Hydrogenation of Penta-Graphene Leads to Unexpected Large Improvement in Thermal Conductivity, Nano Lett. 16 (2016) 3925–3935.

[50] H.L. Kagdada, S.D. Dabhi, P.K. Jha, Bandgap tuning and enhancement of Seebeck coefficient in one dimensional GeSe, AIP Conf. Proc. 1942 (2018) 110010.

[51] V. Sharma, H.L. Kagdada, P.K. Jha, P. Śpiewak, K.J. Kurzydłowski, Halogenation of SiGe monolayers: robust changes in electronic and thermal transport, Phys. Chem. Chem. Phys. 21 (2019) 19488–19498.

[52] H.L. Kagdada, P.K. Jha, P. Śpiewak, K.J. Kurzydłowski, D.K. Singh, Pressure-induced first order phase transition in bulk GeSe, J. Appl. Phys. 127 (2020) 175104.